This is a preprint, the final version is subject to change, of the American Mineralogist (MSA)
Cite as Authors (Year) Title. American Mineralogist, in press.
DOI: https://doi.org/10.2138/am-2018-6608

REVISION #1

Structural variations along the apatite F-OH join

JOHN M. HUGHES[1,4*], DANIEL HARLOV[2,3], JOHN F. RAKOVAN[4]

[1]Department of Geology, University of Vermont, Burlington, Vermont, 05405, U.S.A.

[2]GeoForschungsZentrum Potsdam, Telegrafenberg, D-14473 Potsdam, Germany

[3]Department of Geology, University of Johannesburg P.O. Box 524, Auckland Park, 2006 South Africa

[4]Department of Geology and Environmental Earth Sciences, Miami University, Oxford, Ohio 45056, U.S.A.

ABSTRACT

The atomic arrangements of eight synthetic samples along the fluorapatite-hydroxylapatite join were examined using X-ray crystallographic techniques; the results of those refinements demonstrate that the incorporation of both F and OH in the apatite anion column, mimicking the human apatite system as modified by fluoridation, is complex. The compositions of the anion columns in the phases ranged from $[F_{0.40}(OH)_{0.60}]$ to $[F_{0.67}(OH)_{0.33}]$, and the high-precision structure refinements yielded *R1* values from 0.0116 to 0.0140. The apatite structure responds to the variable content of the anion columns. Counterintuitively, the OH groups in the anion column move monotonically closer to the mirror planes at z = 1/4, 3/4 with increasing F content, despite the decreasing size of the triangle of Ca2 atoms to which the column anions bond and the increasing overbonding of the hydroxyl oxygen. In the structure the F atoms are underbonded and have zero degrees of positional freedom in the (0,0,1/4) special position to relieve that underbonding; the bonding deficiency of the anion column is relieved by the

overbonding of the O(H) atom in the anion column, overbonding that increases with increasing content of underbonded F in the anion column. Together the underbonded F and the overbonded OH meet the formal bond valence (1.0 *vu*) required by the anion column occupants. The changes in bonding from the individual anion column occupants to the surrounding Ca2 atoms with composition induce bond length changes principally in the irregular Ca2 polyhedron, and also affect the *a* lattice parameter in the apatites. The bond valence values imparted on the F, OH column anions, when extrapolated to end-member compositions, suggest that different column anion arrangements may exist near the F and OH endmember compositions, as is also seen along the apatite Cl-OH join. These values have implications for the incorporation of fluoride in human teeth during the fluoridation process.

INTRODUCTION

Apatite *sensu lato* is the most abundant phosphate mineral on Earth, and is fundamentally important in geology, materials science, biology, medicine, agriculture and dentistry. The mineral serves as the base of the phosphorus cycle on our planet. Apatite is employed in many geological applications, including several different geochronology and thermochronology techniques (Chew and Spikings 2015). Apatite is also a major repository of halogens in rocks of the Earth's crust and mantle (Piccoli and Candela 2002; Harlov and Aranovich 2018). Because of its robust atomic arrangement, apatite is also host to many substituents (Hughes and Rakovan 2015), making it an oft-used tool in geochemical studies.

Apatite has many industrial applications as well. The phase has emerged as an important tool in environmental remediation through PIMS (*P*hosphate *I*nduced *M*etal *S*tabilization; Wright and Conca 2002). Apatite is also used in radionuclide sequestration, as its Ca1 and Ca2 sites serve as a solid-state repository for radioactive substituents (Ewing and Wang 2002; Rakovan and

Pasteris 2015). Apatite was historically heavily used in the fluorescent lighting industry (Hughes 2015). Apatite is also used as a lasing material; through co-doping of substituents in the Ca1 and Ca2 sites, "designer" apatite lasers can be manufactured with desirable optical properties (Payne et al. 1994). Each Li-Fe-Phosphate battery in an electric car consumes 60 kg of P mined principally from apatite (Elser et al. 2012). In addition, approximately 80 million metric tons of phosphoric acid worldwide are produced annually for many industrial uses (European Phosphate Fertilizer Alliance 2018; 2015 data).

The most important use of apatite is as a source of phosphorus for fertilizer. The dramatic rise in world population in the twentieth century was enabled by a parallel dramatic rise in apatite mining for fertilizer manufacturing to feed the growing world population; the coincidence of world population and "phosphate rock" (apatite) production is illustrative of the societal importance of apatite (Hughes 2015). Worldwide, apatite consumption, dominantly for use as fertilizer, is approximately 20 kg apatite•yr^{-1} per capita (Etter et al. 2011).

Except for small portions of the inner ear, all hard tissue of the human body is formed of apatite materials, indicating the remarkable link between geology and biology for the mineral; apatite is among the most common biominerals on Earth. Significant research has been undertaken on the nature of bone and tooth apatite, and recent breakthroughs in characterizing bone apatite chemistry have been made (Pasteris et al. 2014). Apatite is also being investigated as a tool to distinguish calcifications that are associated with benign and malignant breast tumors in a non-invasive manner (Kerssens et al. 2010), and is also used as a coating on prostheses inserted into human bone to improve the rate of bone-prosthesis melding and speed healing (Constantz and Osaka 1994).

The U.S. Centers for Disease Control and Prevention has named the bioengineering of fluorine addition to natural hydroxylapatite in teeth as one of the ten greatest public health achievements of the twentieth century. In research recounted in Hughes (2015), it was discovered in the early 1900s that addition of small amounts of fluorine to the hydroxylapatite of natural teeth made them much more resistant to dental caries, thus leading to fluoridation of nearly ¾ of U.S. water supplies in a public health undertaking.

Apatite is thus one of the most important mineral phases on Earth, and for this reason the phase has been extensively studied. Recent detailed summaries of the crystal chemistry and materials applications of apatite can be found in Hughes (2015) and the entire *Elements* volume devoted to the mineral (Harlov and Rakovan 2015).

The basic apatite atomic arrangement is well known, but the details of anion compatibility in the apatite anion column are not as well understood. In the tripartite apatite anion solid solution series (fluorapatite, hydroxylapatite, chlorapatite), the three phases are distinguished by the dominant anion species in the [00*z*] anion column. Any solid solution between two end-members or among the three end-members of the anion solid solution must account for steric interactions between or among the anions that occupy the anion column in that apatite.

Despite its fundamental importance in inorganic and organic systems, the mechanism(s) and extent of solid solution between and among the hydroxylapatite, fluorapatite, and chlorapatite end-members are only now being elucidated. The nature and extent of solid solution among these endmembers is extremely important because many material properties in the apatite system are dependent upon anion composition and structure of the apatite phase. The column anion arrangement of natural ternary apatites was first elucidated by Hughes et al. (1990), who showed that the seemingly incompatible F, OH, and Cl can all be

accommodated in a single anion column with the creation of new column anion sites that are not seen in the individual endmembers. They also showed that both hexagonal and monoclinic variants of natural ternary apatites exist. Hughes et al. (2014a, 2014b) demonstrated that in both synthetic and natural samples along the fluor-chlorapatite join, solid solution is attained by creation of a novel, off-mirror fluorine site not seen in any other apatite. Hughes et al. (2016) examined the atomic arrangement of synthetic apatites along the chlor-hydroxylapatite join, and showed that the compatibility of the two anions is complex, and three different column anion arrangements exist, arrangements that are dependent on the Cl-OH composition of the apatite. Kelly et al. (2017) subsequently showed that these variants in anion column arrangement do occur in nature. The final apatite binary, the F-OH apatite join, is examined in this paper.

As noted previously, fluoridation of tooth apatite has been named one of the ten greatest public health achievements of the twentieth century. Surprisingly, however, there are no known structure studies of phases along the fluor-hydroxylapatite binary, and thus the method of accommodation of solid solution has not been elucidated. We here present high-precision atomic arrangements of eight synthetic F-OH apatite samples, devoid of the steric constraints of substituent Cl. The X-ray study illustrates the structural adjustments required to accommodate both F and OH in the apatite anion column.

EXPERIMENTAL

Synthesis of apatite samples

Apatites across the F-OH join were synthesized utilizing F-OH exchange between synthetic pure end member fluorapatite and a series of $Ca(OH)_2$-H_2O solutions at 1100 °C and

400 MPa. Synthesis of a large size range of fluorapatite crystals up to 5 or more mm in length was achieved by dry mixing 0.03 moles (9.3 grams) of $Ca_3(PO_4)_2$ into 0.1 moles of CaF_2 (11 grams). This mix was taken up to 1375 °C in a covered Pt crucible in open air, soaked at 1375 °C for 15 hours, and then slowly cooled to 1220 °C at 3 °C per hour after which the crucible was removed from the oven and air cooled (see Schettler et al. 2011). The fluorapatite crystals were released from the flux by boiling the crystal/flux mass in 2 liters of a 20% $Al(NO_3)$ solution followed by 3 or 4 additional washings in distilled (Millipore) water.

Apatites across the F-OH join were then synthesized by exchanging 400 mg of a 200 – 500 μm size separate of these synthetic fluorapatites with 100 – 300 mg of a $Ca(OH)_2$-H_2O solution with variable proportions of $Ca(OH)_2$ and H_2O. Each of the fluorapatite-$Ca(OH)_2$-H_2O mixes were sealed in a 4 cm long, 5 mm diameter Pt capsule and taken up to 1100 °C and 400 MPa in an internally heated gas pressure vessel using Ar as the pressure medium. Run duration was 3 – 6 days. The temperature was measured with 3 S-type thermocouples and calibrated based on measurements of the melting points of NaCl at 843 °C/200MPa and 904 °C/500 MPa (Akella et al. 1969). The accuracy is about ± 5 °C at 200 MPa and ± 20 °C at 500 MPa. Maximum thermal gradients along the capsules were ± 10 °C. Pressure measurement was undertaken with a strain gauge and was accurate to ± 7 MPa for experiments up to 500 MPa. During the experiment, pressure was controlled automatically within ± 5 MPa using the hydraulic system of the intensifier and a programmable control unit. The samples were heated isobarically with a rate of 30 °C/min and quenched isobarically with quench rates of 150–200 °C/min.

During the experiment the following total exchange took place between the fluorapatite crystals and the $Ca(OH)_2$-H_2O solution *via* a coupled dissolution-reprecipitation process (see Putnis 2009):

$$Ca_5(PO_4)_3F + Ca(OH)_2 = Ca_5(PO_4)_3(F,OH) + CaF_2 \quad (1)$$

and

$$Ca_5(PO_4)_3F + H_2O = Ca_5(PO4)_3(F,OH) + HF \quad (2)$$

After quench the Pt capsule was opened and the exchanged F-OH apatites removed and washed 4 – 5 times in a 100 ml beaker of doubly distilled H_2O at room temperature to remove the CaF_2, HF, and the remaining $Ca(OH)_2$. The washed F-OH apatite crystals were then air-dried at room temperature.

X-ray structure studies

X-ray diffraction data were collected with a Bruker Apex II CCD single-crystal diffractometer using graphite-monochromated Mo K_α radiation; complete details of crystal data and data collection, results of the structure studies, and cif files for each of the eight synthetic crystals described herein have been deposited.[1] For each sample, data were collected for a redundant sphere of reciprocal space (average redundancy ≈ 16) and were integrated and corrected for Lorentz and polarization factors and absorption using the Bruker Apex2 package of programs. The atomic arrangement was refined in space group $P6_3/m$, on F^2, with SHELXL-97

[1] Deposit items AM-19-xx1 for crystal data and data collection conditions, AM-19-xx2 for positions of atoms and equivalent isotropic atomic displacement parameters, and AM-19-xx3 for CIF files, respectively. Deposit items are available two ways: for paper copies contact the Business Office of the Mineralogical Society of America (see inside front cover of recent issue) for price information. For an electronic copy visit the MSA web site at http://www.minsocam.org, go to the *American Mineralogist* Contents, find the table of contents for the specific volume/issue wanted, and then click on the deposit link there.

(Sheldrick 2008) using neutral atom scattering factors and full-matrix least-squares, minimizing the function $\Sigma\, w(F_o^2 - F_c^2)^2$ with no restraints. All atoms were refined with anisotropic temperature factors except the column anions; an extinction coefficient was also refined. After initial refinements of the structure, the column anion positions were located using difference maps. In earlier studies it was found that the use of anisotropic atomic displacement factors for the column anions yields unreasonable values of U_{33}, an anisotropy that masks the positions of anion sites occupied by small fractions of a column anion (Hughes et al. 2016). The occupancy values of the column anions were not constrained, as discussed subsequently in the chemistry section.

Chemistry

The chemistry of the synthetic apatite phases was analyzed through crystal structure analysis. The crystals were synthesized using pure reagents in the Ca-P-O-F-H system; during the structure refinement all sites save the column anion sites were assumed to be fully occupied, an assumption supported by testing release of occupancy factors; the superior final *R*1 values ($0.0116 \leq R1 \leq 0.0140$) in the final structure refinements also corroborated that assumption. The column anions are assumed to sum to 2.00 *apfu*, as required for charge balance. The experimentally determined sum of column anions, determined without constraints or restraints, yielded the range $2.04\ apfu \leq [F + O(H)] \leq 2.08\ apfu$; the slight deviation from the ideal value of 2.00 *apfu* (2 - 4%) may result from the use of neutral-atom scattering factors rather than partially or fully ionized scattering factors. We believe these analyses obtained by site-occupancy refinement are at least as accurate and precise as electron microprobe measurements of F and the calculation of O(H) by difference (Hawthorne and Grice 1990; Stormer et al. 1993;

Stock et al. 2015; Kelly et al. 2017). The results of the column anion composition by site refinement are given in Table 1.

RESULTS

The Cl, F, and OH anions in apatite exist in [00*z*] anion columns at the edges of the unit cell. Those columns intersect two mirror planes in the apatite $P6_3/m$ unit cell, at $z = ¼$ and $z = ¾$. The anion column intersects each mirror plane in the center of an equilateral triangle of three Ca2 atoms, with adjacent Ca2 triangles (along *c*) ½ unit cell above or below being rotated by 60° by the 6_3 screw axis (Figure 1). Because of the disparate size of the three column anions, steric constraints exist on their coexistence in the anion column, and those constraints have been the subject of extensive study (Hughes and Rakovan 2015). Although the natural "end-members" of hydroxylapatite and fluorapatite may contain small amounts of Cl in the anion column, the synthetic samples described herein are devoid of Cl, and thus only record the interactions between OH and F in the anion column.

The fluorine atom in apatite is of the ideal size to fit centered in the triangle of the Ca2 atoms (Figure 1), and thus it is located coplanar with the triangle, within the mirror planes at $z = ¼, ¾$ in the unit cell. The hydroxyl, however, is slightly larger, and is displaced approximately 0.35 Å above or below the center of the triangle (Figure 1), half-occupying 0,0,*z* positions on the $z = ¼$ mirror plane at approximately 0,0,0.20 and 0,0,0.30 (and 0,0,0.70 and 0,0,0.80 at the mirror plane at $z = ¾$). The much larger Cl atom, not present in samples in this work, occupies half-occupied positions approximately 1.2Å above or below the mirror plane. The following summarize the structural relationships that arise in the central portion of the fluorapatite-hydroxylapatite solid solution series.

204

205 **Lattice parameters and column anion composition**

206 The column anion occupants of apatite do not control the *c* lattice parameter in calcium
207 phosphate apatites (R^2 = 0.0199 for the relationship between composition and the *c* lattice
208 parameter). Indeed, the F, OH and Cl calcium phosphate apatite with the *largest* anion occupant,
209 chlorapatite, has the *smallest c* lattice parameter (Hughes and Rakovan 2002; fluorapatite, *c* =
210 6.8782Å, hydroxylapatite, *c* = 6.875Å, and chlorapatite, *c* = 6.774Å). However, the column anion
211 occupants are highly correlated with the *a* lattice parameter. Figure 2 depicts the relationship
212 between F content in the anion column and the *a* lattice parameter among the synthetic F-OH
213 apatites studied herein, and demonstrates the high positive correlation between the OH content of
214 the anion column and *a* lattice parameter (R^2 = 0.9756).

215

216 **O(H) position and column anion composition**

217 Figure 3 displays the relationship between the *z* value of the O(H) in the anion column
218 and the fluorine content of the anion column, and demonstrates the high correlation (R^2 =
219 0.9832). The relationship demonstrates that the hydroxyl position in fluor-hydroxylapatite is not
220 static; as the amount of column F increases, the hydroxyls in the column monotonically shift
221 toward their associated mirror plane at *z* = ¼ or ¾.

222

223 **Area of Ca2 triangle and column anion composition**

224 The Ca2-Ca2 distance, and thus the area of the Ca2 triangle in fluor-hydroxyl apatite,
225 responds to the substitution of OH and F in the fluor-hydroxylapatite anion column. Figure 4

demonstrates that with increasing F in the anion column the area of the Ca2-Ca2-Ca2 triangle in the (0,0,1/4) and (0,0,3/4) mirror planes monotonically decreases (R^2 = 0.9914).

Ca2 bond lengths to column anions and column anion composition

The column anions in apatite bond to the Ca2 atoms in the triangle surrounding the anion column. The equivalent distances to the three Ca2 atoms in the studied apatites varies systematically as a function of F content of the anion column. Figure 5 displays the Ca2-F distance in the fluor-hydroxyl apatites. Also depicted are the bond strengths of those bonds, which are a function of the bond length (Brese and O'Keeffe 1991). As shown in that figure, the Ca2-F bond length decreases monotonically with increasing F substitution in fluor-hydroxylapatite (R^2 = 0.9917), and the bond strength of those bonds concomitantly increases (R^2 = 0.9903; although bond length and bond strength are not linear functions, over this relatively narrow range of bond distances they approximate a linear function). Similarly, with increasing F content in the fluor-hydroxylapatite anion column, the Ca2-O(H) bond length also decreases monotonically (Figure 6; R^2 = 0.9831), and the Ca2-O(H) bond strengths increase concomitantly (R^2 = 0.9888).

Inductive changes to polyhedral bonds and column anion composition

The column anions in calcium phosphate apatites are in the first coordination sphere only for the Ca2 atoms, save for any hydrogen bonding in the column anion itself. The substitution of OH and F in the hydroxylapatite anion column induces changes in bond lengths principally within the Ca2 polyhedron. In addition to the column anion, the Ca2 atom bonds to one O1 atom,

one O2 atom, and four O3 atoms (2 x O3, 2 x O3'), and monotonic bond length changes are induced in each of those bonds with varying F and OH content in the anion column.

Figure 7 depicts the changes in Ca2 bond lengths with O1 and O2 in the fluor-hydroxylapatite series studied herein. As seen in that figure, The Ca2-O1 bond lengths decrease systematically with increasing F in the anion column of fluor-hydroxylapatite, with $R^2 = 0.9813$. Conversely, the Ca2-O2 bond length increases monotonically with an increase in F in these fluor-hydroxylapatites ($R^2 = 0.9922$). For the Ca2-O3 bonds (x2; Figure 8), the bond length increases over a small range (range < 0.003Å; $R^2 = 0.9016$) with increasing F content of the fluor-hydroxylapatite anion column, whereas for the Ca2-O3' bonds (x2) the bond length increases with increasing F content ($R^2 = 0.9892$; Figure 8).

The transmission of bond length changes to second-coordination sphere polyhedra with changing F/OH composition in the anion column is not as pervasive as the first-coordination sphere discussed above. For the Ca1 polyhedron, the Ca1-O1 (x3) bond length has a high negative correlation with F content ($R^2 = 0.9600$; not pictured), whereas the Ca1-O2 (x3) and Ca1-O3 (x3) bonds are not well-correlated with anion column composition (R^2 values = 0.0795 and 0.0745 respectively). Similarly, the bond-length variations are also not transmitted to the rigid phosphate tetrahedron, with R^2 values for P-O1, -O2, and –O3 (x2) = 0.0161, 0.0336, and 0.1216, respectively.

DISCUSSION OF THE ATOMIC ARRANGEMENT IN FLUOR-HYDROXYLAPATITE

The results of the high-precision studies on apatites in the middle range of the fluor-hydroxylapatite binary are of interest because they elucidate changes in the apatite structure that allow for the continuous solid solution between these two end-member compositions, and have

implications for the stability of different compositions along the join. In previous studies involving Cl-bearing synthetic apatites (Hughes et al. 2014b, 2016), the incompatibility of the larger Cl atom and the smaller F atom and OH group yielded previously unknown mechanisms for accommodating the size disparity in the column anions. The like-sized OH and F were expected to yield a simple solid solution, but many aspects of the solid solution are counterintuitive.

In the F-OH apatites, the anion column occupants control the *a* lattice parameter, with *a* increasing with increasing OH in the anion column (Fig. 2). In the calcium phosphate apatites, the F, Ca2, P, O1 and O2 atoms are located within the (00z) mirror planes at $z = ¼$ and ¾. As OH increases and the area of the Ca2 triangle expands within the (0,0,1/4) and (0,0,3/4) mirror planes, the unit cell expands in (001), as evidenced in the monotonic increase of the *a* lattice parameter with [OH]. As the column anion occupants only bond to atoms within the mirror plane (non-hydrogen bonding), there is essentially no relation between the amount of any column anion and the *c* lattice parameter.

The *z* parameter of the column OH varies monotonically with OH content, with the hydroxyl moving closer to the mirror planes at $z = ¼, ¾$ with increasing F content (Fig. 3). Such movement is counterintuitive. As the Ca2 triangle expands with increasing OH in the anion column, maintenance of bond valence would suggest that the OH would move *toward* the mirror plane to maintain its bond distance and bond valence (1.00 *vu*) with its three symmetrically equivalent bonds to Ca2 atoms. However, the converse is true, as the O(H) migrates monotonically *away from* the mirror plane with *increasing* OH (and concomitantly decreasing F), and the reason is subtly obvious. The F atom in the (0,0,1/4 and 0,0,3/4) special position has no degrees of positional freedom, and as the Ca2 triangle expands with increasing OH the F atom

loses bond valence, as its position is fixed. The OH column occupants must thus contribute their own 1.0 valence unit *and,* by overbonding, account for the deficiency of Ca2-F bond valence to the anion column if bond valence thereto is to be maintained at 1.0 *vu*. Consequently, with an increasing portion of F in the anion column (and concomitant shrinking Ca2 triangle), the OH must make up increasing bond valence lost by the F atoms collectively. Thus the hydroxyl migrates closer to the mirror plane to account for its bond valence as well as the bond-valence deficiency that increases with increasing F content because of the greater proportion of underbonded fluorine. It does so efficiently, as the bond valence sum to the anion column at each mirror plane averages 0.985 *vu*, with a range from 0.955 to 0.997 *vu*, in the compositions studied.

The bonding of the Ca2 atoms to the column anions in F-OH apatite is of interest because it has implications for the stability of different compositions along the F-OH join. The bond distances and bond-valence values between the three Ca2 atoms in the Ca2 triangle and the column F atom are depicted in Figure 5. As shown therein, the Ca2-F distance varies monotonically with the F content in the anion column controlled by the expansion of the Ca2 triangle by the insertion of hydroxyls in the anion column. As also shown, the bond valence between the Ca2 atoms and the F atoms varies between ~0.26 and ~0.29 *vu*, demonstrating that in all compositions the F atom is underbonded as it bonds to the three symmetry equivalent Ca2 atoms in the triangle, yielding 0.78 to 0.87 *vu* bond sums to the F atom. The F atom is in a (0,0,1/4) special position, and if it was to move off that position it would become even more underbonded.

The underbonding to the anion column that results from the Ca2-F bonds must be accommodated by the bonds between Ca2 and OH. Figure 6 displays the bond lengths and bond strengths between the Ca2 atoms in the Ca2 triangle and the OH in the anion column. There is a

monotonic change in bond length with F-OH composition, with decreasing Ca2-O(H) bond length with increasing F in the anion column. The reason for that decreasing bond length is revealed in the bond-valence values of each Ca2-O(H) bond. In all cases the column hydroxyl is overbonded, and the overbonding of O(H) increases with increasing F. As noted above, this increased overbonding results from the underbonding that occurs between each F atom and Ca2 atoms, and the total underbonding thus increases with increasing F content. That underbonding to the column F atoms is compensated by overbonding to the O(H) atoms, yielding total bonding to the anion column near 1.00 *vu*.

Finally, there are inductive effects throughout the Ca2-O_6X (X = F, O(H)) polyhedron that result from the changes in bond valence from the column anions. Figures 7 and 8 illustrate the monotonic change in bond distances between the Ca2 atoms and the oxygen atoms of its first coordination sphere. The bond lengths from Ca2 to O1, O2, O3 and O3' are depicted, and display monotonic variations with F content in the anion column of F-OH apatite. The varying bond lengths serve to balance the bond strength variation from the column anions, as the bond valence sums for the Ca3 atoms in the structures studied vary between 1.97 and 1.99 *vu*.

IMPLICATIONS

We have successfully synthesized crystals with compositions along the middle portion of the F-OH apatite join, and undertaken high-precision crystal structure refinements of the synthesis products. The results of those refinements demonstrate that the incorporation of both F and OH in the apatite anion column, mimicking the human apatite system as modified by fluoridation, is complex because of the lack of positional degrees of freedom of the F atoms. The results also suggest implications for those regions of the binary that have yet to be studied.

As seen in Figure 9, in the compositional region studied, the F atoms in the anion column are underbonded, with the total underbonding to the anion column increasing with the amount of F in the column. The O(H) in the column is overbonded, with the overbonding increasing with increasing F in the column. The two affects counterbalance; the total bond valence sum to the column ranges from 0.955 to 0.997 *vu*, demonstrating the reason for the counterintuitive behavior of the O(H) column anion.

The introduction of fluoride *via* drinking water and other methods has proven highly effective in the reduction of dental caries. There are several mechanisms by which fluoride acts to decrease caries, including inhibition of hydroxylapatite dissolution (demineralization) through the formation of surface complexes, enhancement of new apatite growth (remineralization), and inhibition of bacterial activity (Featherstone 1999). Until this work, however, the atomic arrangement of the anion column occupants along the F-OH binary was unknown.

We are currently undertaking experiments to synthesize the remaining regions of the F-OH join; the implications of this study suggest those compositions are particularly important. As deduced from Figure 9, if the bond valence sums for O(H) are projected to a composition of $F_{2.00}$ (i.e., the bonding incident upon the first hydroxyl substituent in a column of pure fluorapatite), the bond valence sum is 1.27 *vu*, and the bonding incident upon the first fluorine substituent in a column of pure hydroxylapatite is 0.70 *vu*. Thus, in a projection of the apatite anion column arrangements to end-member compositions, the first F substituent is dramatically underbonded in hydroxylapatite and the first OH substituent is dramatically overbonded in fluorapatite, by amounts that may not allow a stable structure. This could have significant effects on the nature of new tooth apatite formed during remineralization in the presence of fluoride. For example it may result in a heterogeneous column anion chemistry with domains of F-rich hydroxylapatite. This

363 may also explain why dissolution and reprecipitation is the main mechanism for substitution of F
364 in to tooth apatite. Alternatively, it has been found that in the Cl-OH binary (Hughes et al. 2016),
365 solid solution is attained by creation of three different, compositionally dependent anion column
366 arrangements along the binary, and the bond-valence values above suggest multiple
367 arrangements may also occur along the F-OH binary to alleviate the underbonding (F) and
368 overbonding (OH) of column constituents. Such possible arrangements would have large
369 implications for fluoridation of hydroxylapatite in the human system.
370

371 **ACKNOWLEDGEMENTS**

372 Support for this work was provided by the National Science Foundation through grants NSF-
373 MRI 1039436 and EAR-1249459 to JMH and EAR-0952298 to JR. The manuscript was
374 improved by reviews by Francis McCubbin and Adrian Fiege. The authors greatly appreciate the
375 editorial handling by AE Aaron Celestian.
376
377

REFERENCES CITED

Brese, N.E., and O'Keeffe, M. (1991) Bond-valence parameters for solids. Acta Crystallographica, B47, 192-197.

Chew, D.M., and Spikings, R.A. (2015) Geochronology and thermochronology using apatite: time and temperature, lower crust to surface. Elements, 11, 189-194.

Constantz, B.R., and Osaka, G.C. (1994) Hydroxyapatite prosthesis coatings. U.S. Patent 5279831 A.

Elliot, J.C. (2002) Calcium phosphate biominerals. *In* Kohn, M., J.F. Rakovan, and J.M. Hughes, Eds., Phosphates: Geochemical, Geobiological and Materials Importance, 48, p. 427–454. Reviews in Mineralogy and Geochemistry, Mineralogical Society of America, Chantilly, Virginia.

Elser, J., Metson, G., and Bennet, E. (2012) Uncertain supplies, shifting demands, and the sustainability of the human phosphorus cycle. 9th INTECOL International Wetlands Conference, Orlando, Florida.

Etter, B., Tilley, E., Khadka, R., and Udert, K.M. (2011) Low-cost struvite production using source-separated urine in Nepal. Water Research, 45, 852–862.

European Phosphate Fertilizer Alliance (2018) Phosphorus: A Key to Life (Data and Statistics). http://aeep.eu/data-and-statistics/phosphoric-acid/, July, 2018.

Ewing R.C., and Wang, L. (2002) Phosphates as nuclear waste forms. Reviews in Mineralogy and Geochemistry 48, 673-700.

Featherstone J. D. (1999) Prevention and reversal of dental caries: role of low level fluoride. Community Dentistry and Oral Epidemiology, 27:31-40.

Harlov, D. E., and Rakovan, J.F. (2015) Apatite: A Mineral for All Seasons. *Elements*, 11, no. 3.

Harlov, D. E. and Aranovich, L., Eds. (2018) The Role of Halogens in Terrestrial and Extraterrestrial Geochemical Processes: Surface, Crust, and Mantle. Springer Geochemistry, 1030 pps.

Hawthorne, F.C., and Grice, J.D. (1990) Crystal-structure analysis as a chemical analytical method: application to light elements. The Canadian Mineralogist, 28, 693-702.

Hughes, J.M. (2015) The many facets of apatite. Mineralogical Society of America Presidential Address. American Mineralogist, 100, 1033-1039.

Hughes, J. M., M. Cameron and K. D. Crowley (1990) Crystal structures of natural ternary apatites: solid solution in the $Ca_5(PO_4)_3X$ (X = F, OH, Cl) system. American Mineralogist, 75, 295-304.

Hughes, J.M., Harlov, D., Kelly S.R., Rakovan, J., and Wilke, M. (2016) Solid solution in the apatite OH-Cl binary system: compositional dependence of solid solution mechanisms in calcium phosphate apatites along the Cl-OH binary. American Mineralogist, 101, 1783-1791.

Hughes, J.M., Heffernan, K.M., Goldoff, B., and Nekvasil, H. (2014a) Fluor-chlorapatite, devoid of OH, from the Three Peaks Area, Utah: The first reported structure of natural fluor-chlorapatite. Canadian Mineralogist, 52, 643-652 (appeared April, 2015).

Hughes, J.M., Nekvasil, H., Ustunisik*, G., Lindsley, D.H., Coraor, A.E., Vaughn*, J., Phillips, B., McCubbin, F.M., and Woerner, W.R. (2014b) Solid solution in the fluorapatite - chlorapatite binary system: High-precision crystal structure refinements of synthetic F-Cl apatite. American Mineralogist, 99, 369-376.

Hughes, J.M. and J. Rakovan (2002) The Crystal Structure of Apatite, $Ca_5(PO_4)_3(F,OH,Cl)$. *In* Kohn, M., J.F. Rakovan and J.M. Hughes, Eds. (2002) *Phosphates: Geochemical,*

Geobiological and Materials Importance, Chapter 1. Mineralogical Society of America Reviews in Mineralogy Series.

Hughes, J.M., and Rakovan, J. (2015) Structure, chemistry, and properties of apatite and apatite supergroup minerals. Elements, 11, 165-170.

Kelly, S., Rakovan, J. and Hughes, J. M. (2017) Column Anion Arrangements in Chemically Zoned Chlorapatite and Fluorapatite from Kurokura, Japan. American Mineralogist, 102, 720-727.

Pasteris, J.D., Yoder, C.H., and Wopenka, B. (2014) Molecular water in nominally unhydrated hydroxylapatite: The key to a better understanding of bone material. American Mineralogist, 99, 16–27.

Payne, S.A., DeLoach, L.S., Smith, L.K., Kway, W.L., Tassano, J.B., Krupke, W.F., Chai, B.H.T., and Loutts, G. (1994) Ytterbium-doped apatite-structure crystals: A new class of laser materials. Journal of Applied Physics, 76, 497–503.

Piccoli, P.M., and Candela, P.A. (2002) Apatite in igneous systems. *In* Kohn, M., J.F. Rakovan and J.M. Hughes, *Eds. Phosphates: Geochemical, Geobiological and Materials Importance*, Chapter 6. Mineralogical Society of America Reviews in Mineralogy and Geochemistry 48, 255-292.

Rakovan, J.F., and Pasteris, J.D. (2015) A technological gem: materials, medical, and environmental mineralogy of apatite. Elements, 11, 195-200.

Stock, M.J., Humphreys, M.C.S., Smith, V.C., Johnson, R.D., Pyle, D.M., and EIMF (2015) New constraints on electron beam induced halogen migration in apatite. American Mineralogist, 100, 281–293.

Stormer, J.C., Pierson, M.L., and Tacker, R.C. (1993) Variation of F and Cl X-ray intensity due to anisotropic diffusion in apatite during electron microprobe analysis. American Mineralogist, 78, 641–648.

U.S. Centers for Disease Control and Prevention (1999) Ten great public health achievements—United States, 1900–1999. Morbidity and Mortality Weekly Report, 48(12), 241–243.

Wright, J., and Conca, J. (2002) Remediation of groundwater and soil contaminated with metals and radionuclides using apatite II, a biogenic apatite mineral. In Extended Abstracts of the 2002 American Chemical Society Meeting, August 18–22, American Chemical Society, Columbus, Ohio.

This is a preprint, the final version is subject to change, of the American Mineralogist (MSA)
Cite as Authors (Year) Title. American Mineralogist, in press.
DOI: https://doi.org/10.2138/am-2018-6608

Table 1. Unconstrained and normalized anion column compositions for F-OH apatites, as determined by X-ray site refinement.

Sample	Unconstrained Anion Comp.	Normalized Anion Comp.
APS68	$[F_{0.66(5)}(OH)_{0.38(6)}]_{\Sigma 1.04}$	$[F_{0.63}(OH)_{0.37}]_{\Sigma 1.00}$
APS69	$[F_{0.48(3)}(OH)_{0.55(4)}]_{\Sigma 1.03}$	$[F_{0.47}(OH)_{0.53}]_{\Sigma 1.00}$
APS70	$[F_{0.45(3)}(OH)_{0.58(4)}]_{\Sigma 1.03}$	$[F_{0.44}(OH)_{0.56}]_{\Sigma 1.00}$
APS77	$[F_{0.41(3)}(OH)_{0.61(3)}]_{\Sigma 1.02}$	$[F_{0.40}(OH)_{0.60}]_{\Sigma 1.00}$
APS84	$[F_{0.59(4)}(OH)_{0.45(3)}]_{\Sigma 1.04}$	$[F_{0.57}(OH)_{0.43}]_{\Sigma 1.00}$
APS85	$[F_{0.45(3)}(OH)_{0.57(4)}]_{\Sigma 1.02}$	$[F_{0.44}(OH)_{0.56}]_{\Sigma 1.00}$
APS86	$[F_{0.63(4)}(OH)_{0.41(4)}]_{\Sigma 1.04}$	$[F_{0.61}(OH)_{0.39}]_{\Sigma 1.00}$
APS87	$[F_{0.70(5)}(OH)_{0.34(6)}]_{\Sigma 1.04}$	$[F_{0.67}(OH)_{0.33}]_{\Sigma 1.00}$

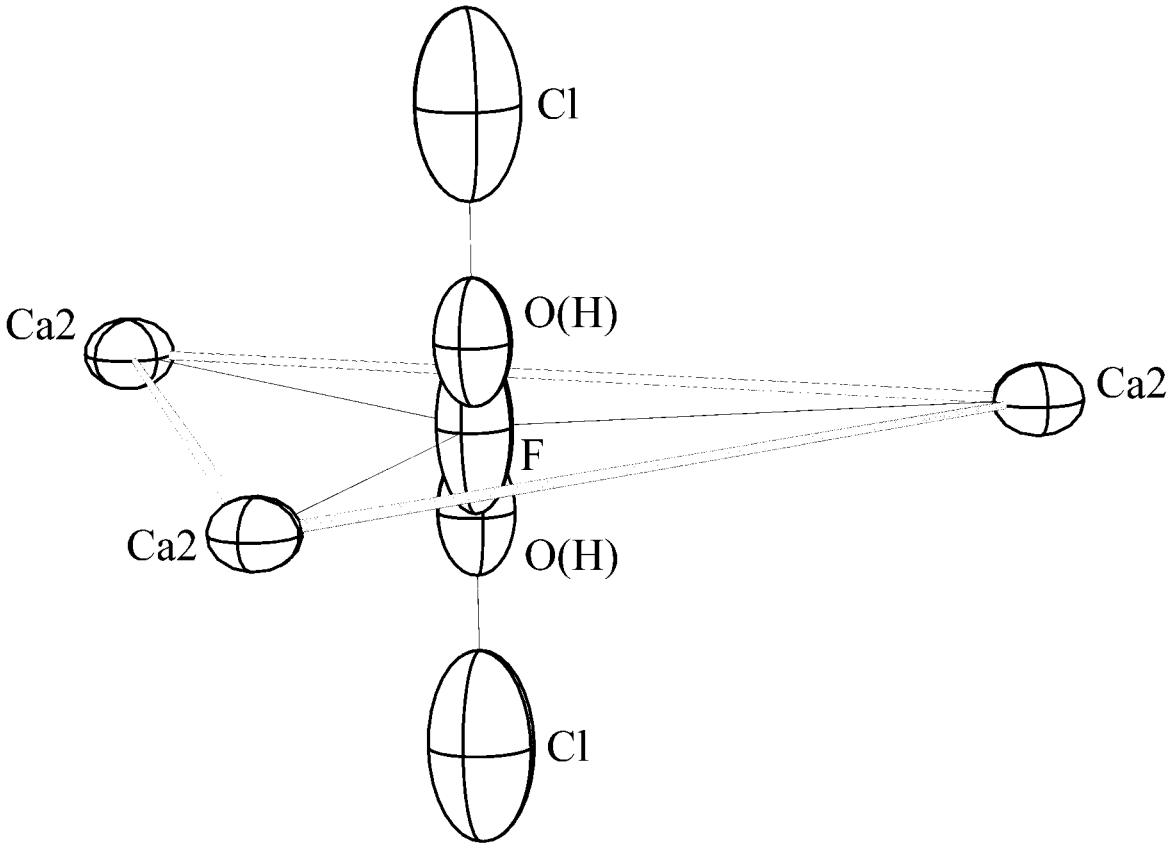

Figure 1. Depiction of location of column anions (Cl, OH, F) in $P6_3/m$ calcium phosphate apatites. The triangle of Ca2 atoms is a mirror plane at z = ¼, ¾. At any one mirror plane, one of the five possible sites is occupied. In the synthetic samples in this paper, only the O(H) and F sites are occupied (from Hughes 2015).

NOTE TO EDITORS: THIS FIGURE TAKEN FROM HUGHES (2015); COPYRIGHT OWNED BY *American Mineralogist*.

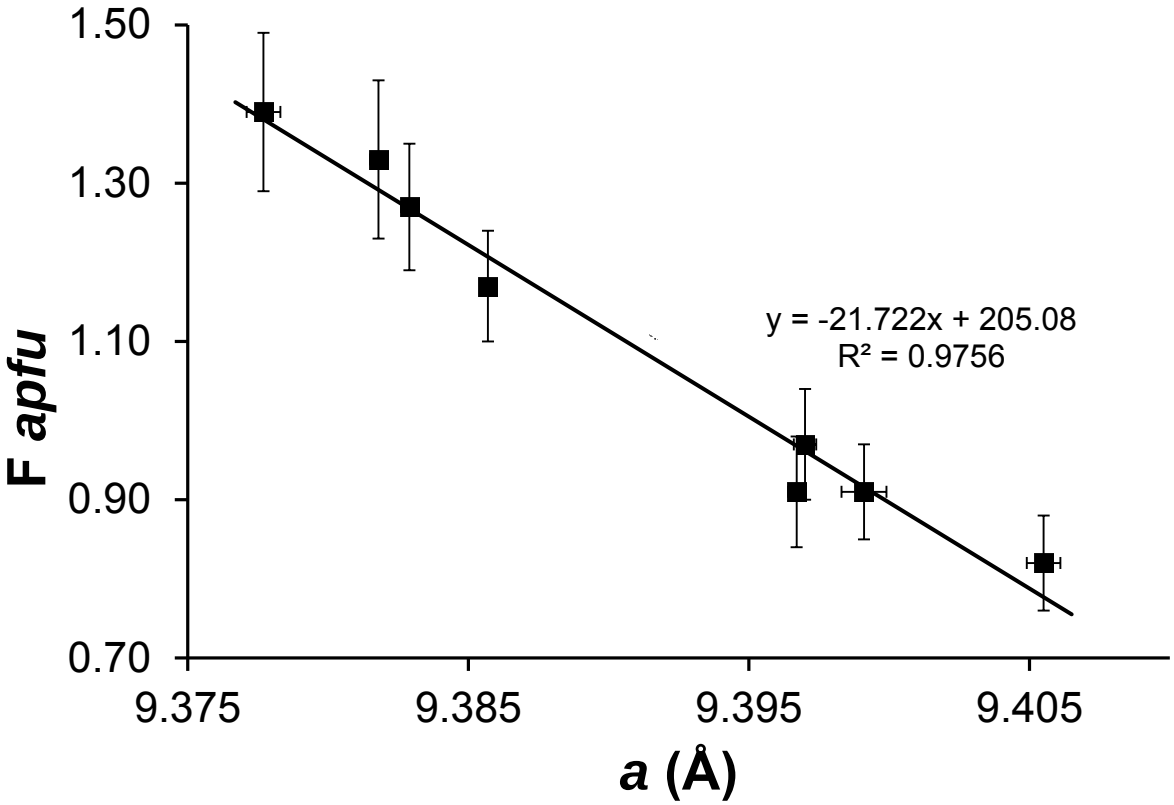

Figure 2. Variation of the fluorine content of the anion column with the *a* lattice parameter; error bars represent one estimated standard deviation (esd).

This is a preprint, the final version is subject to change, of the American Mineralogist (MSA)
Cite as Authors (Year) Title. American Mineralogist, in press.
DOI: https://doi.org/10.2138/am-2018-6608

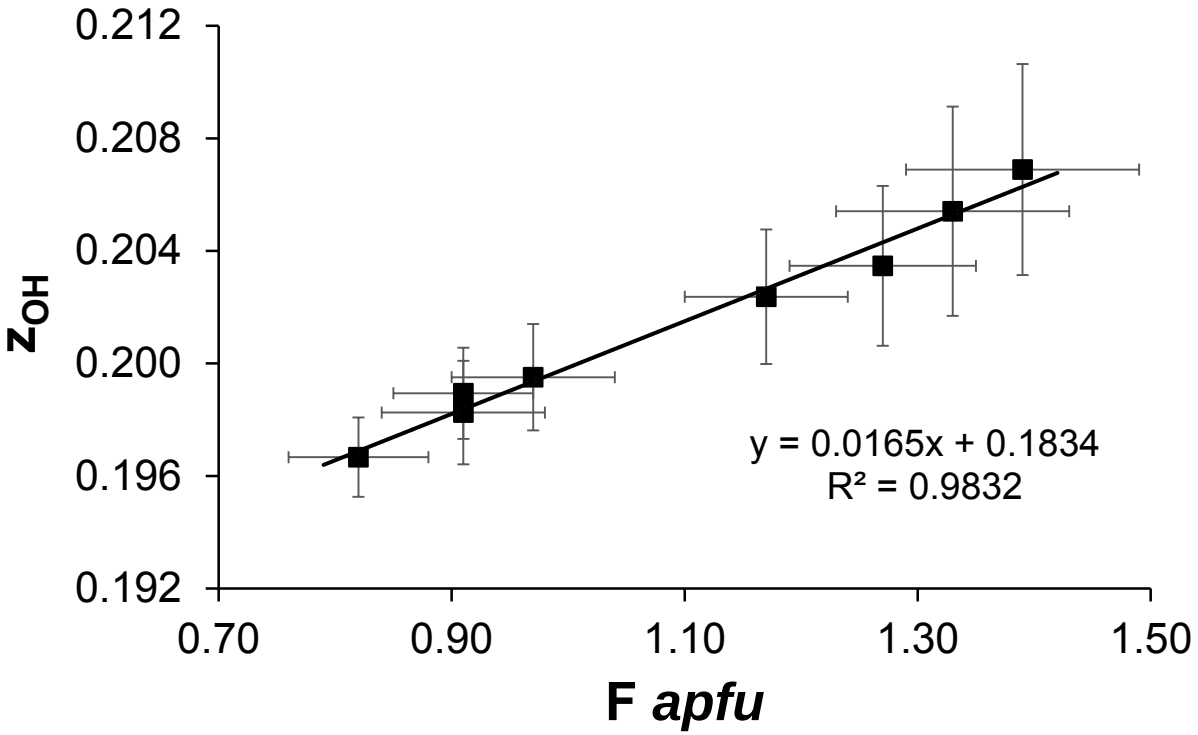

Figure 3. Variation of the *z* parameter of the anion column hydroxyl with fluorine content of the anion column; error bars represent one esd.

This is a preprint, the final version is subject to change, of the American Mineralogist (MSA)
Cite as Authors (Year) Title. American Mineralogist, in press.
DOI: https://doi.org/10.2138/am-2018-6608

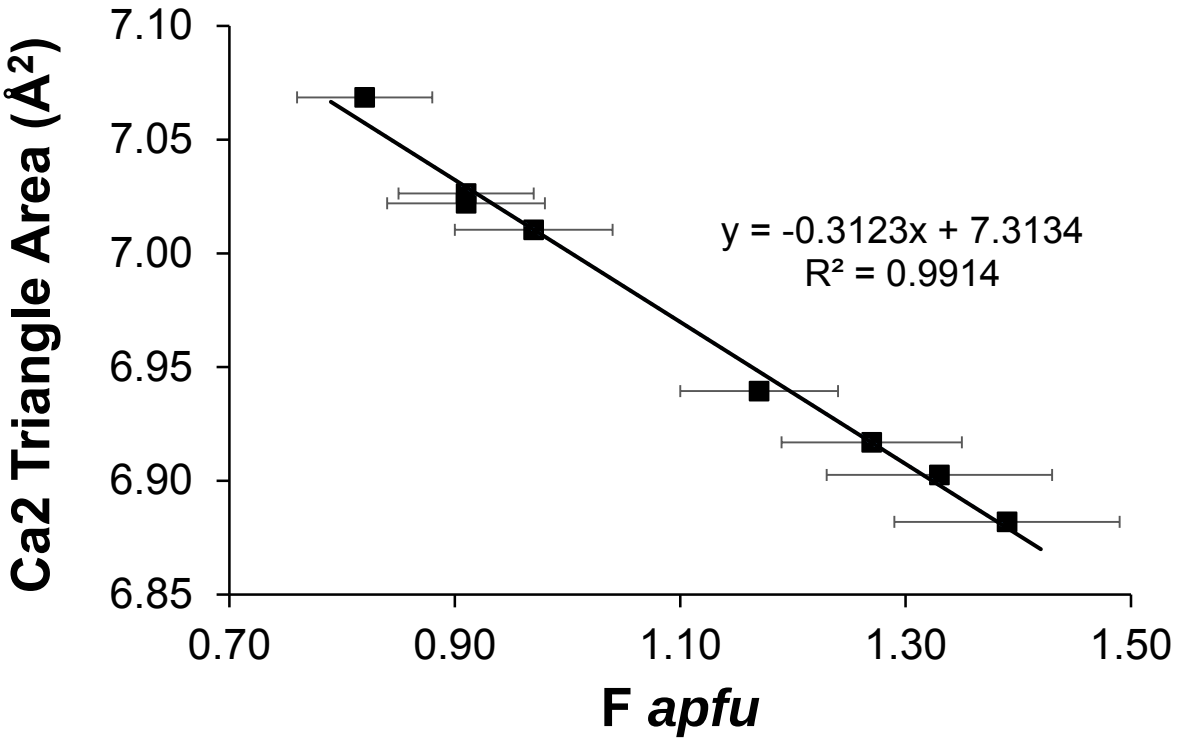

Figure 4. Variation of the area of the Ca2 triangle with fluorine content of the anion column; error bars represent one esd.

504

505

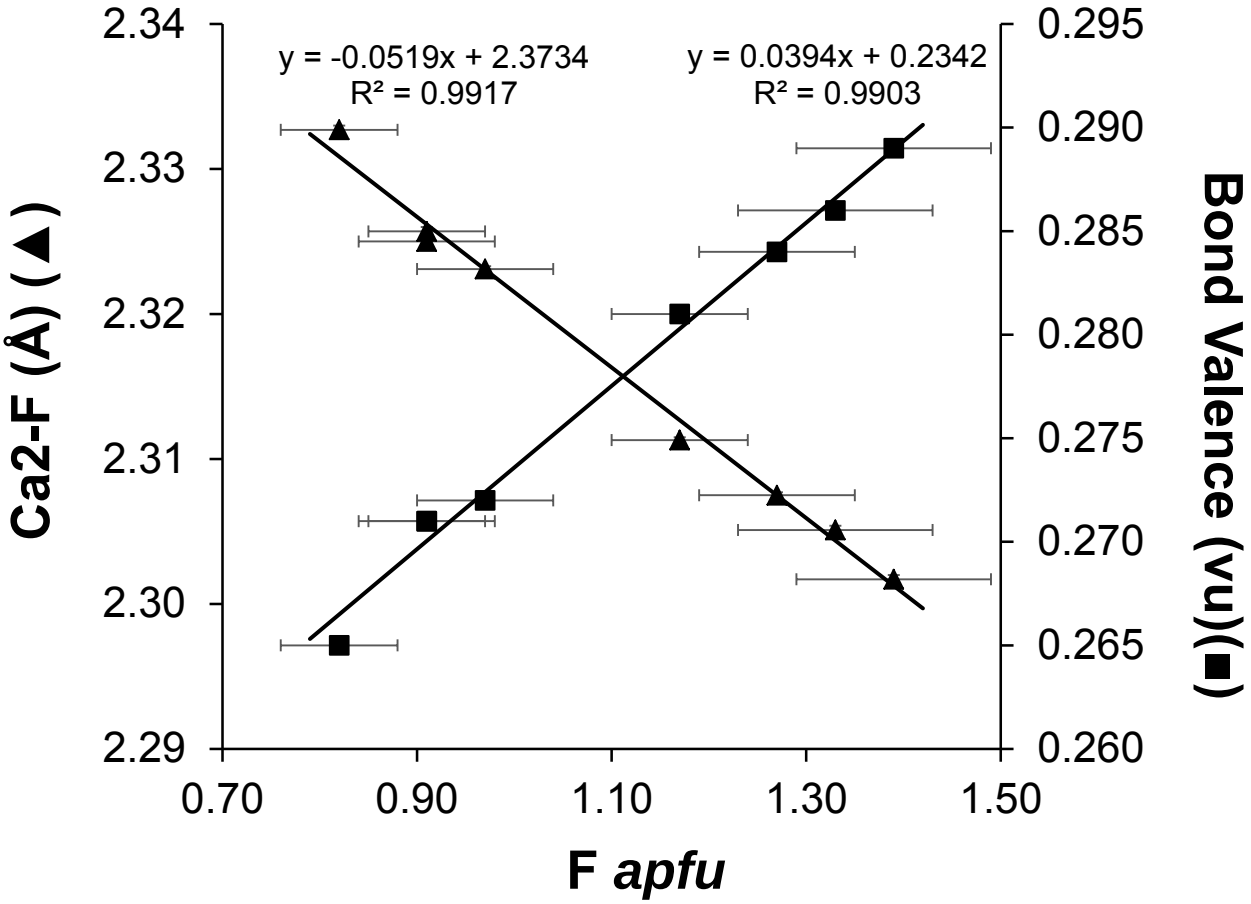

506

507

508 **Figure 5**. Variation of Ca2-F bond lengths (triangles) and bond valence (squares) with
509 fluorine content of the anion column; error bars represent one esd. Vertical error bars for bond
510 lengths are contained within data points. Vertical error bars for bond valence not included.

511

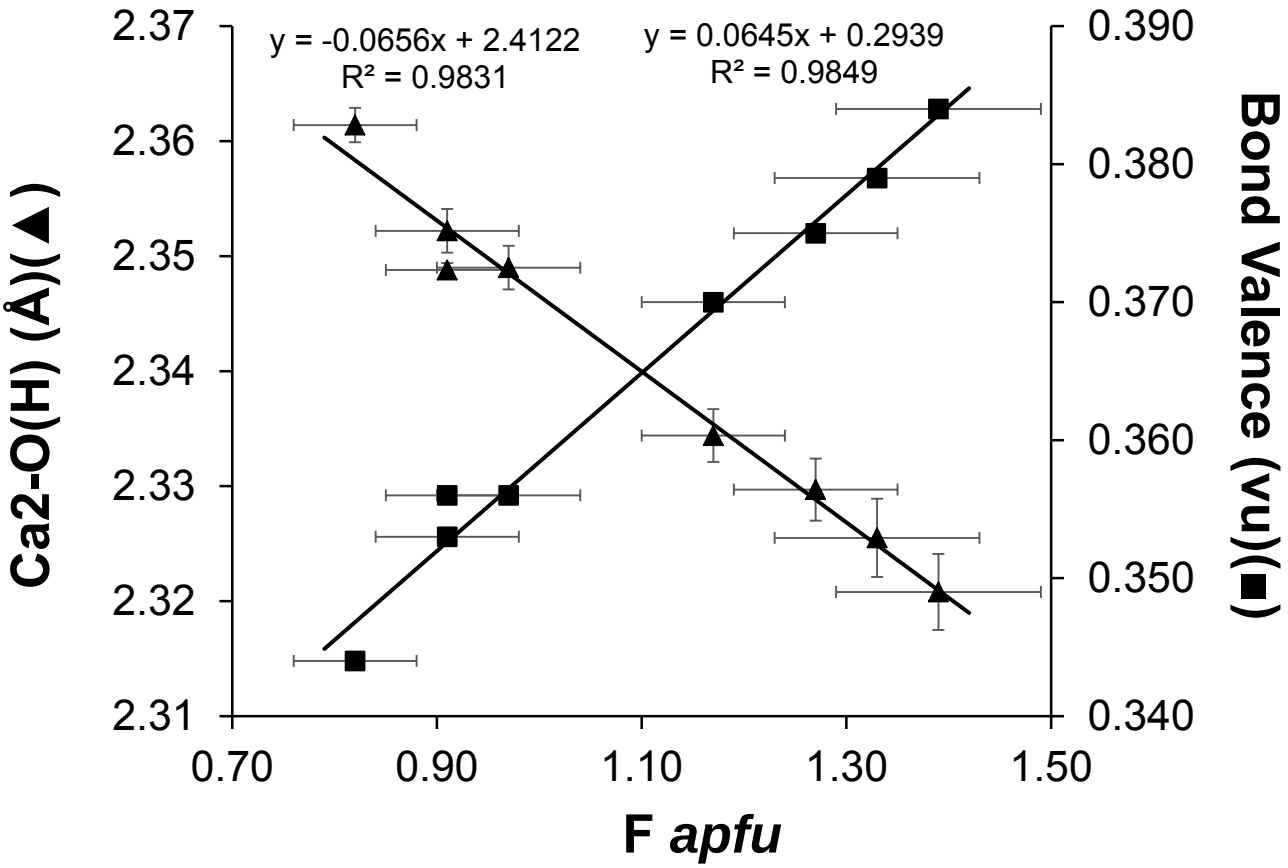

Figure 6. Variation of Ca2-O(H) bond lengths (triangles) and bond valence (squares) with fluorine content of the anion column; error bars represent one esd. Vertical error bars for bond valence not included.

This is a preprint, the final version is subject to change, of the American Mineralogist (MSA)
Cite as Authors (Year) Title. American Mineralogist, in press.
DOI: https://doi.org/10.2138/am-2018-6608

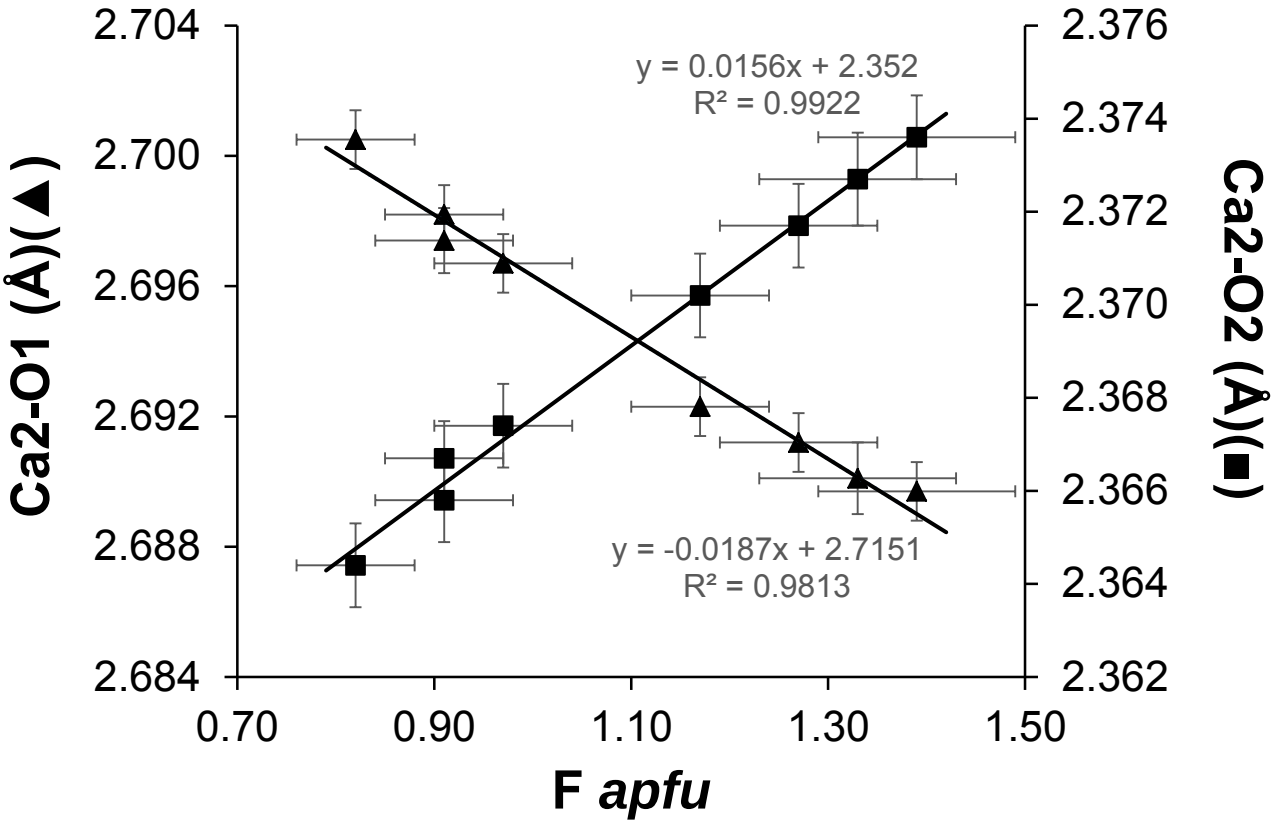

Figure 7. Ca2-O1 (triangles) and Ca2-O2 (squares) bond length variations with column anion composition in fluor-hydroxylapatite.

This is a preprint, the final version is subject to change, of the American Mineralogist (MSA)
Cite as Authors (Year) Title. American Mineralogist, in press.
DOI: https://doi.org/10.2138/am-2018-6608

529

530

531

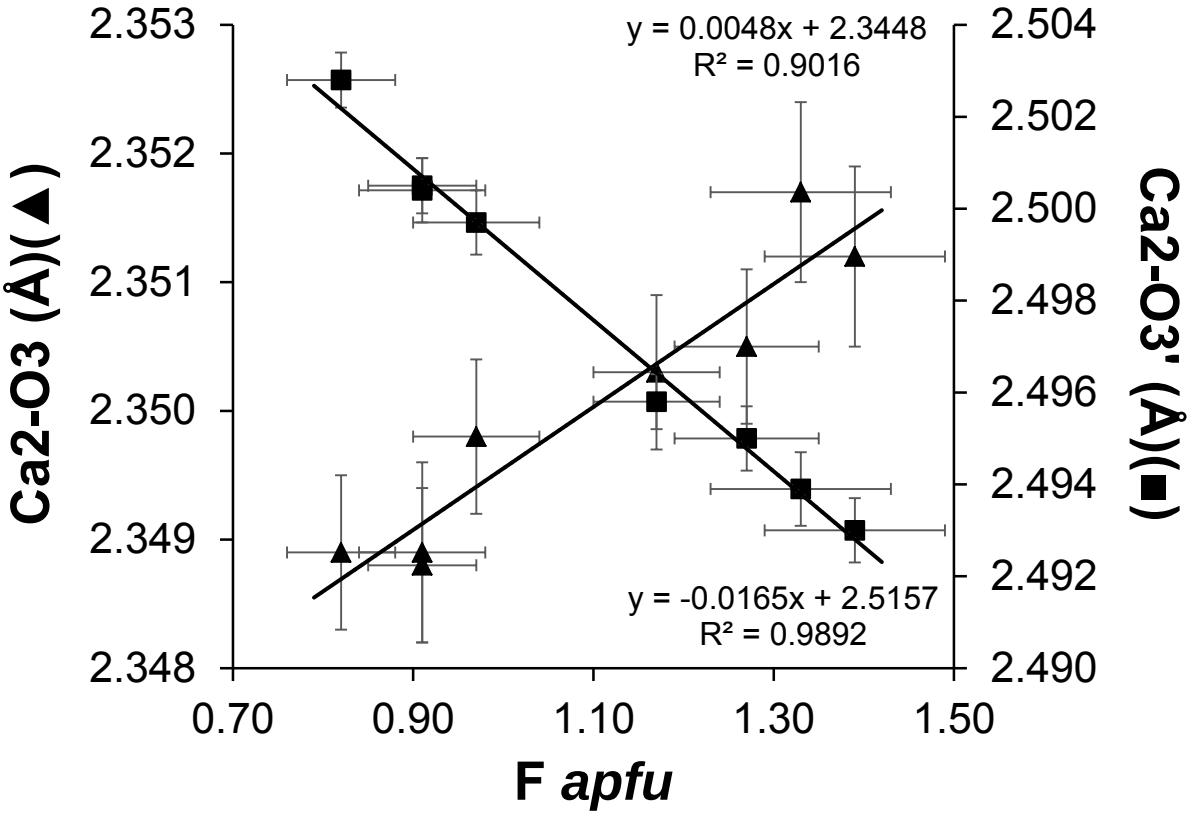

532

533 **Figure 8**. Ca2-O3 (triangles) and Ca2-O3' (squares) bond length variations with column

534 anion composition in fluor-hydroxylapatite.

535

536

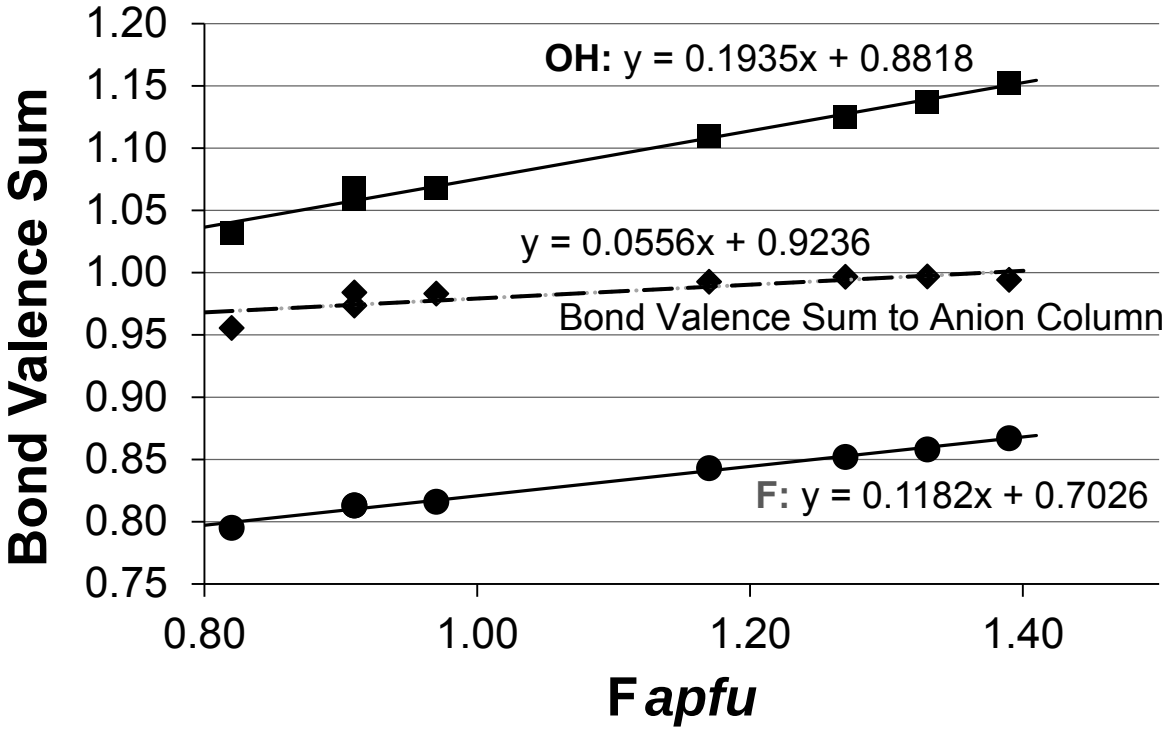

537

538 **Figure 9**. Bond valence to O(H) and F and bond-valence sum to anion column for the
539 specific samples examined in this study.

540